GLOBAL BIOGEOCHEMICAL CYCLES, VOL. 13, NO 3, PAGES 785-802, SEPTEMBER 1999

The substitution of high-resolution terrestrial biosphere models and carbon sequestration in response to changing CO_2 and climate

Robert Meyer[1], Fortunat Joos[1], G. Esser[2], M. Heimann[3], G. Hooss[4], G. Kohlmaier[5], W. Sauf[4], R. Voss[4], U. Wittenberg[2]

Abstract. Strategies are developed to analyze and represent spatially resolved biosphere models for carbon sequestration in response to changes in atmospheric CO_2 and climate by reduced-form, substitute models. We explore the High-Resolution Terrestrial Biosphere Model as implemented in the Community Terrestrial Biosphere Model (HRBM/CTBM), the Frankfurt Biosphere Model (FBM), and the box-type biosphere of the Bern model. Storage by CO_2 fertilization is described by combining analytical representations of (1) net primary productivity (NPP) as a function of atmospheric CO_2 and (2) a decay impulse response function to characterize the timescales of biospheric carbon turnover. Storage in response to global warming is investigated for the HRBM/CTBM. The relation between the evolution of radiative forcing and climate change is expressed by a combination of impulse response functions and empirical orthogonal functions extracted from results of the European Center/Hamburg (ECHAM3) coupled atmosphere-ocean general circulation model. A box-type, differential-analogue substitute model is developed to represent global carbon storage of the HRBM/CTBM in response to regional changes in Temperature, Precepitation and cloud cover. The substitute models represent the spatially resolved models accurately and cost-efficiently for carbon sequestration in response to changes in CO_2 or in CO_2 and climate and for simulations of the global isotopic signals. Deviations in carbon uptake simulated by the spatially resolved models and their substitutes are less than a few percent.

1. Introduction

Complex models with high spatial resolution representing the terrestrial carbon cycle [e.g., *Cao and Woodward*, 1998; *Esser*, 1987; *Haxeltine and Prentice*, 1996; *Heimann*, 1998; *Janecek et al.*, 1989; *McGuire et al.*, 1992; *Melillo et al.*, 1993; *Potter et al.*, 1993; *Prentice et al.*, 1992], the oceanic carbon cycle [e.g., *Maier-Reimer and Hasselmann*, 1987; *Sarmiento et al.*, 1992; *Orr*, 1999], or the coupled atmosphere-ocean climate system [e.g., *Kattenberg et al.*, 1996] are used to simulate the links between anthropogenic carbon emissions, the oceanic and terrestrial carbon sinks, atmospheric CO_2, and global warming. Simulations with complex, spatially resolved models require a considerable amount of computing time, which, in practice, limits their application. However, once complex models or model components have been developed, the potential exists to represent their behavior by reduced-form, substitute models (SMs). Recently, the traditional linear impulse response function approach [e.g., *Siegenthaler and Oeschger*, 1978; *Oeschger and Heimann*, 1983; *Maier-Reimer and Hasselmann*, 1987; *Sarmiento et al.*, 1992; *Enting et al.*, 1994; *Hasselmann et al.*, 1996] has been extended to include nonlinear elements [*Joos et al.*, 1996; *Joos and Bruno*, 1996; *Thompson and Randerson*, 1999; *Hooss et al.*, 1999] to permit applications of SMs over a wider range of boundary conditions. SMs

[1]Physics Institute, University of Bern, Bern, Switzerland
[2]Institute for Plant Ecology, Justus-Liebig-Universität, Giessen, Germany
[3]Max-Planck-Institut fuer Biogeochemie, Jena, Germany
[4]Max-Planck-Institut fuer Meteorologie, Hamburg, Germany
[5]IPTC, J.W. Goethe Universität, Frankfurt am Main, Germany

Paper number 1999GB900035
0886-6236/99/1999GB900035$12.00

of the complex models are not intended to capture all aspects of complex models, but they are intended as convenient and cost-efficient tools to represent the complex models' response to changes in certain key variables. SMs can also be combined to a comprehensive, albeit simplified, models of the Earth system.

SMs permit important calculations and provide valuable insights. Key processes are described in a compact form that simplifies their analysis [e.g., *Joos et al.*, 1996; *Bolker et al.*, 1998; *Thompson and Randerson*, 1999]. Nonlinear SMs of the carbon cycle have been applied in Monte Carlo analyses to assess the uncertainties in reconstructions of the oceanic and terrestrial carbon sinks based on the atmospheric CO_2 and $\delta^{13}C$ record [*Bruno and Joos*, 1997; *Indermühle*, 1999; *Joos et al.*, 99 a]. The Monte Carlo analyses have required simulations of several million model years that would not have been feasible with a complex model. SMs of the carbon cycle and the climate system were coupled to formulations describing the economic system in integrated assessment studies to investigate optimal emission pathways [e.g., *Hasselmann et al.*, 1996; *Joos et al.*, 99 b]. Such optimizations require many model iterations, which would be prohibitively expensive with complex models. Nonlinear SMs have been used for projections of future atmospheric CO_2 and global warming from anthropogenic carbon emissions requiring the coupling of biogeochemical and climate model components [*Joos and Bruno*, 1996; *Schimel et al.*, 1996; *Schimel et al.*, 1997; *Hooss et al.*, 1999].

Nonlinear SMs have been developed for a hierarchy of ocean carbon cycle models [*Joos et al.*, 1996; *Hooss et al.*, 1999]. However, nonlinear SMs of terrestrial carbon cycle models are scarce [*Joos et al.*, 1996; *Thompson and Randerson*, 1999]. To fill this gap, we present in this paper SMs for the spatially resolved High-Resolution Biosphere Model (HRBM) [*Esser*, 1987; *Esser*, 1991; *Esser et al.*, 1994; *Wittenberg and Esser*, 1997; *Heimann*, 1998; *Kicklighter*, 1999] and the Frankfurt Biosphere Model (FBM) [*Janecek et al.*, 1989; *Kindermann*, 1993; *Kohlmaier*, 1997; *Kohlmaier et al.*, 1998; *Lüdeke*, 1994; *Lüdeke et al.*, 1995]. In addition, we will compare our results with those obtained with the box-type biosphere of the Bern model [*Siegenthaler and Oeschger*, 1987; *Siegenthaler and Joos*, 1992; *Joos et al.*, 1996]. In this article, we show that terrestrial models can be simplified drastically while preserving their essential dynamics. We represent the response of a spatially resolved model to changes in CO_2 and climate by a few equations only and validate the SMs for all the characteristic timescales of the model.

Terrestrial carbon storage is influenced by a number of processes that interact in a complex way [*Schimel et al.*, 1994 a, b]. The interplay between deforestation and land use changes, increasing atmospheric CO_2, nutrient availability, climate change, the frequency of fires and other disturbances, species composition feedback and other factors modify terrestrial carbon storage. The models included in the present study are of intermediate complexity in that many of these processes are represented only in a highly parameterized form. Nevertheless, the models are able to simulate the basic features of the terrestrial carbon cycle (e.g. the large scale geographic distribution of Net Primary Productivity (NPP) [*Cramer et al.*, 1999] and terrestrial carbon stocks, seasonal cycle of carbon exchanges [*Heimann*, 1998; *Nemry et al.*, 1999], and uptake of excess carbon induced by the rise in atmospheric CO_2 [*Kicklighter*, 1999]). Models that describe the terrestrial processes more comprehensively are presently still under development. For example, first results with dynamic vegetation models that address the species composition feedbacks are just emerging (http://www.pik-potsdam.de/posters.htm).

In this study, we consider carbon storage in response to increasing CO_2 and climate only. The CO_2 fertilization effect is the dominant process for the sequestration of anthropogenic carbon in the considered models in which biome composition and distribution are kept constant. For example, projected changes in climate offset the carbon sequestration due to CO_2 fertilization by ~20% in the HRBM/CTBM for a scenario where atmospheric CO_2 is quadrupled and temperature increased by 5°C relative to the preindustrial level.

Our strategy to map the spatially-resolved HRBM and FBM models builds upon the following elements: (1) In a first step, we consider terrestrial carbon uptake in response to rising CO_2 only. This allows us to apply a nonlinear impulse response technique that was previously used to build SMs for ocean carbon models and box-type terrestrial models [*Joos et al.*, 1996]. (2) We reformulate the SM based on an impulse response function as a box-type differential-analogue model to map the response in carbon storage of the spatially resolved HRBM/CTBM to both increasing CO_2 and climate change (temperature, precipitation, and cloudiness). (3) We apply empirical orthogonal functions (EOFs) and principal components (PCs) extracted from a scenario run with the European Center/Hamburg Model 3 /Large Scale Geostrophic coupled (ECHAM3/LSG) atmosphere-ocean general circulation model (AOGCM) [*Hooss et al.*, 1999] to determine the relation between radiative forcing, climate change, and terrestrial carbon storage.

1. The dynamics of a linear and time-invariant system are fully characterized by its impulse response function (IRF) (also termed pulse response function, Green's function, kernel function, or fundamental solution). The biospheric response to CO_2 fertilization is dictated by the increase in primary productivity and

the timescales of carbon overturning. For constant climate conditions, terrestrial carbon overturning is often described by linear or approximately linear functions of carbon stocks. Therefore its dynamics can be captured by an IRF. On the other hand, primary productivity depends in a nonlinear way on atmospheric CO_2. Combining both the IRF and the nonlinear productivity function as determined from the spatially resolved models yields an impulse response function substitute model (IRF SM) for CO_2 fertilization.

The impulse technique has distinct advantages. It provides quantitative measures to analyze key terrestrial processes for carbon sequestration and to compare and evaluate the dynamics of terrestrial models on a global scale. We provide simple analytical functions for the dependence of primary productivity on atmospheric CO_2 and for the IRFs that qualify the timescales of carbon overturning (see *Bolin and Rodhe* [1973] for an overview).

2. Changes in temperature T, and precipitation P affect local and global respiration in a nonlinear way. Thus, under changing climate, the respiration is not simply a linear function of carbon stocks and the IRF concept is not applicable. In order to circumvent this limitation, we mapped the spatially resolved HRBM/CTBM onto a global box model. Thereby the dependence of respiration on the T and P fields is approximated by rate coefficients that depend exponentially on global average surface temperature. This approach yields an effective global Q_{10} factor as a measure for the decrease in the average overturning time of the total carbon stock. The effective Q_{10} factor results from all the local grid-cell responses in productivity and respiration to local changes in the climate variables.

3. The spatiotemporal response of an AOGCM to an increase in radiative forcing can be captured by a combination of IRFs [*Joos and Bruno*, 1996; *Hasselmann et al.*, 1996] that takes into account the inertia of the climate system and EOFs that describe the spatial patterns of climate change [*Hooss et al.*, 1999]. Such a representation provides a simple approximation to the results of the spatially resolved AOGCM that can be easily incorporated into SMs. Here we have applied results of *Hooss et al.* [1999] to force the HRBM/CTBM biota model to investigate its response to climate change.

In conclusion, our attempt is to build biospheric SMs that are simple, cost-efficient, and accurate representations of the spatially resolved model for terrestrial carbon storage by CO_2 fertilization and carbon release in response to global warming.

2. Model Description

2.1. Nonlinear Biospheric IRF Substitute Model

To introduce the basic IRF concept, we consider first the substitution of a simple linear differential-analogue model. The box model may represent, for example, a grid cell of the spatially resolved model or the global land biota. The net flux of carbon into the biosphere $f_{ab,\mathrm{net}}$, i.e., net ecosystem production (NEP), is viewed as the difference between the flux into the biosphere by primary productivity, f_{prod}, and the flux leaving the biosphere due to respiration of organic material, f_{resp}, that may also include the oxidation of organic matter by fire. We subtract the steady state fluxes and consider the perturbations relative to steady state as indicated by the Δ symbol:

$$f_{ab,\mathrm{net}} = \Delta f_{\mathrm{prod}} - \Delta f_{\mathrm{resp}} \tag{1}$$

We use a "decay" IRF, r_{decay}, to describe how long assimilated carbon remains in the biosphere and to calculate the respiration flux. Given a unit δ impulse of carbon input at time t', the value of r_{decay} after some time interval $t - t'$ is the fraction of the impulse that is currently being released at time t. The functional form of r_{decay} can be obtained simply by monitoring the model's respiration of carbon that was added by such an impulse to the assimilating pools. The box model can be substituted by

$$f_{ab,\mathrm{net}}(t) = \Delta f_{\mathrm{prod}}(t) - \int_{t_0}^{t} \Delta f_{\mathrm{prod}}(t') r_{\mathrm{decay}}(t - t') dt' \tag{2}$$

In practice, the integral describing respiration is solved as a sum using time intervals dt' of 1 year, thereby neglecting seasonality. Then, the annual decay at year t is the sum of all earlier (surplus) annual productions $\Delta f_{\mathrm{prod}}(t')$ that are multiplied by the fraction that is respired at year t, i.e., the value of the decay IRF r_{decay} at age $t - t'$. The time t_0, where the integration is started, refers to a time prior to the first perturbation in productivity, e.g., the preindustrial equilibrium. This approach is exact when the dynamics of internal carbon turnover and respiration are linear and time invariant. The productivity that is usually a nonlinear function, e.g., of atmospheric CO_2, is described by a separate equation.

Equation (2) is also applicable for the carbon isotopes ^{13}C and ^{14}C. For example, the biospheric uptake of radiocarbon is

$${}^{14}f_{ab,net}(t) = \Delta^{14} f_{\mathrm{prod}}(t) - \int_{t_0}^{t} \Delta^{14} f_{\mathrm{prod}}(t')\ e^{-\lambda(t-t')}\ r_{\mathrm{decay}}(t - t')\ dt' \tag{3}$$

Radioactive decay is taken into account in the respiration term; λ is the radioactive decay rate (1/8267 years) for ^{14}C.

The ^{14}C flux into the biosphere, $\Delta^{14} f_{\mathrm{prod}}$, is the product of the ^{12}C flux (f_{prod}), the atmospheric isotopic ra-

tio ${}^{14}R_a$, and the fractionation factor for the photosynthesis process (${}^{14}\alpha_{a,b}$) [*Farquhar et al.*, 1989]. Splitting f_{prod} in an equilibrium flux ($f_{\text{prod},0}$) and a perturbative flux [$\Delta f_{\text{prod}}(t)$] yields

$$\Delta^{14} f_{\text{prod}}(t) = (f_{\text{prod},0} + \Delta f_{\text{prod}}(t))\ {}^{14}\alpha_{a,b}\,{}^{14}R_a(t) - f_{\text{prod},0}\ {}^{14}\alpha_{a,b}\ {}^{14}R_a(t_0) \quad (4)$$

Next, we extend the approach to spatially resolved models. The global perturbation in productivity, ΔF_{prod}, is

$$\Delta F_{\text{prod}}(t) = \sum_i \Delta f_{\text{prod},i}(t) \quad (5)$$

where $\Delta f_{\text{prod},i}$ is the perturbation in primary productivity for grid cell i and the sum is over all grid cells. The global perturbation in respiration, ΔF_{resp}, is defined as the sum over all grid cells of the difference between current and unperturbed (preindustrial) respiration flux:

$$\Delta F_{\text{resp}}(t) = \int_{t_0}^{t} \sum_i \Delta f_{\text{prod},i}(t')\ r_i(t-t')dt' \quad (6)$$

where r_i is the decay IRF for grid cell i. Again, the dynamics of carbon overturning at each grid point are assumed to be (approximately) linear and time invariant. Equation (6) is transformed into the form of (2) by the scale factor ΔF_{prod} representing the perturbation in global primary productivity:

$$\Delta F_{\text{resp}}(t) = \int_{t_0}^{t} \Delta F_{\text{prod}}(t') \left(\sum_i \frac{\Delta f_{prod,i}(t')}{\Delta F_{\text{prod}}(t')} r_i(t-t') \right) dt' \quad (7)$$

$$\approx \int_{t_0}^{t} \Delta F_{\text{prod}}(t') R_{\text{decay}}(t-t')dt' \quad (8)$$

We identify the term in brackets in (7) as the IRF describing global average decay, R_{decay}. R_{decay} is computed as average of the local decay functions weighted by the local relative contributions to the total productivity perturbations, $\Delta f_{\text{prod},i}/\Delta F_{\text{prod}}$ as weights.

In general, productivities and the weights are time dependent. Then, the productivity-weighted global average IRF is not simply a function of the age difference $t - t'$ but also varies through time. However, as long as the relative contributions of local productivity fluxes to the total productivity do not change significantly, (7) can be approximated by using a single global decay IRF, R_{decay}, as shown in (8).

In summary, we will use two elements to build a nonlinear IRF SM for CO_2 fertilization in spatially resolved biota models: (1) a relation linking the global productivity to atmospheric CO_2 and (2) a globally averaged, time-invariant IRF to describe the respirative decay.

2.2. High-Resolution Biosphere Model

The HRBM/CTBM [*Esser et al.*, 1994; *Wittenberg and Esser*, 1997; *Kicklighter*, 1999; *Heimann*, 1998] is an implementation of the successor of the Osnabrück Biosphere Model [*Esser*, 1987, 1991] in the Community Terrestrial Biosphere Mode (W. Sauf, personal communication). The spatial resolution of the HRBM/CTBM is 0.5° × 0.5°, and the temporal resolution is 1 month. Climate forcing is prescribed using mean climatological data for each grid cell (updated from *Leemans and Cramer* [1991]; W. Cramer, personal communication, 1996). Seventeen different types of natural vegetation are considered [*Prentice et al.*, 1992]. Land use and vegetation fires are not considered here.

Net primary productivity (NPP) as modelled in the HRBM/CTBM is a function of atmospheric CO_2, climate, and soil quality [*Esser et al.*, 1982]. NPP depends neither on carbon assimilated during previous years nor on the atmospheric CO_2 history. Thus the same single relation links NPP and atmospheric CO_2 for different atmospheric CO_2 scenarios, as climate is kept unchanged. Decay of organic matter is modeled proportional to the pool sizes with rate coefficients that depend on temperature, precipitation and on the quality of the decomposing material. Thus respiration in the HRBM/CTBM depends linearly on earlier production (as long as no climate variations are considered). Therefore the HRBM/CTBM can be substituted exactly for CO_2 fertilization and constant climate by the IRF SM approach at individual grid cells.

2.3. Frankfurt Biosphere Model

The FBM [*Janecek et al.*, 1989, *Kindermann*, 1993, *Kohlmaier*, 1997, *Kohlmaier et al.*, 1998, *Lüdeke*, 1994, 1995, *Heimann*, 1998, *Kicklighter*, 1999] is a seasonal model with a time step of one day and a spatial resolution of 0.5° × 0.5°. The same climate forcing is used as for the HRBM/CTBM. Thirty-three different types of natural vegetation are considered. Gross primary productivity (GPP) is calculated as a function of photosynthetically active radiation, surface air temperature, soil water availability, leaf area index (LAI), and atmospheric CO_2. The CO_2 dependence of GPP was introduced in accordance with the work of *Kirschbaum* [1993], which itself is based on the biochemical model of photosynthetic CO_2 assimilation in C_3 plants by *Farquhar et al.* [1980]. The LAI is calculated from the carbon inventory in the compartments representing the living biota. Assimilated carbon is allocated in a nonlinear way into these compartments [*Janecek et al.*, 1989]. Autotrophic respiration and litter production depend on temperature and linearly on compartment size. Heterotrophic respiration is computed from soil carbon mass, temperature, and soil moisture.

Unlike for the HRBM, nonlinearities in GPP and allocation permit only an approximate description of an individual grid cell of the FBM by the IRF SM approach. The dependence of GPP on the size of the living biota reservoir implies that the primary productivity flux depends on the amount of carbon allocated in previous years and thus on the atmospheric CO_2 history. Hence a single relation between GPP and actual atmospheric CO_2 concentration as used in the IRF SM is only an approximation. In addition, the ratio of carbon allocated into the different living biota compartments changes with time owing to the complex and nonlinear allocation and phenology schemes implemented in the FBM. Then, a single scenario-invariant IRF will not be able to exactly capture the dynamics of total respiration, because carbon allocated into the compartment for leaves and feeder roots will be respired faster than that allocated into the compartment representing structural material. These nonlinearities in GPP and allocation will make it more difficult to substitute the FBM than the HRBM.

2.4. Bern Model

The biosphere is represented in the Bern model by a global box model [*Siegenthaler and Joos*, 1992; *Joos et al.*, 1996]. It consists of four pools representing ground vegetation, wood, detritus and soil organic carbon [*Emanuel et al.*, 1984; *Siegenthaler and Oeschger*, 1987], with each reservoir having a distinct overturning time of 2.9, 20, 2.2, and 100 years, respectively. NPP depends logarithmically on atmospheric CO_2 [*Enting et al.*, 1994], and the scale factor (β=0.287) of the relation was determined in order to close the carbon budget [*Schimel et al.*, 1996] for the 1980 to 1990 period. NPP for the preindustrial concentration of 278 ppmv is 60 GtC yr^{-1}. The Bern model has been applied for carbon cycle scenario calculations and the determination of global warming potential in various assessments of the Intergovernmental Panel on Climate Change (IPCC) [e.g. *Houghton et al.*, 1996].

2.5. Substitute Representation of Climate Models

For the investigation of the biospheric response to climate change, we need to generate a space-time-dependent signal in those climate variables that are relevant for biospheric carbon storage. This has been done with an IRF-based substitute representation (*Hooss et al.* [1999]) of the ECHAM3/LSG AOGCM at the Max-Planck Institute for Meteorology.

Hooss et al. [1999] have extracted the spatial and temporal evolution of the climate change signal from the AOGCM output by applying an empirical orthogonal function analysis. The perturbation of a climate variable, Δv, is represented as the superposition of a set of mutually orthogonal spatial patterns, $\mathrm{EOF}_i^{\Delta v}(\mathbf{x})$, and the time-dependent scalar coefficients termed principal components, $\mathrm{PC}_i^{\Delta v}(t)$:

$$\Delta v(\mathbf{x}, t) = \sum_i \mathrm{PC}_i^{\Delta v}(t) \cdot \mathrm{EOF}_i^{\Delta v}(\mathbf{x}). \qquad (9)$$

Originally, the EOF analysis is a method to determine the dominant modes of variability in multivariate time series such as generated by climate model simulations. Each of the PC-EOF pairs i is computed from the AOGCM output in successive order to explain the maximum possible variance in a climate variable. In transient climate change simulations, the variance is usually dominated by the emerging anthropogenic signal. Thus the spatiotemporal patterns of climate change in response to anthropogenic greenhouse gas forcing can be approximated by the first few EOFs and PCs.

The EOFs and PCs for near-surface temperature, cloudiness, precipitation, and sea level have been extracted from an 850 year transient AOGCM simulation where atmospheric CO_2 was prescribed to rise exponentially to reach the fourfold of the preindustrial value at model year 120; afterward, CO_2 was kept constant. The control simulation has been subtracted from the transient run; then EOFs and PCs were determined for each climate variable.

According to the findings of *Hooss et al.* [1999], only the first EOF-PC pair of each of the three climate variables showed a long-term trend identifying them as climate change signal. Thus it appears sufficient for this study to compute the climate forcing for the HRBM/CTBM from the first terms only ($\mathrm{PC}_1^{\Delta v}(t)$, $\mathrm{EOF}_1^{\Delta v}(\mathbf{x})$). The first EOF and PC capture 97% of the variability in near-surface temperature, 43% of the variability in cloud cover, and 31% of the variability in precipitation. Thus for temperature almost the entire climate change signal is described by the first EOF and PC alone. On the other hand, cloud cover and precipitation show high spatiotemporal variability and EOF_1 and PC_1 provide a rough estimate how climate change will manifest itself in these high-noise variables. It is noted that changes in the frequency of extreme events such as droughts and other changes in the variability of precipitation and cloud cover not described by the first EOF-PC pair may also play an important role for changes in the biosphere; these changes have not yet been investigated.

For scenario calculations, we project the change in climate variables from the evolution of CO_2 and radiative forcing. Radiative forcing (in W per m^2) is assumed to depend logarithmically on CO_2 [*Shine et al.*, 1990]. The inertia of the climate system is captured by IRFs. For example, the IRF for temperature describes the evolution of global average surface temperature for a step increase in forcing [*Hooss et al.*, 1999]. Then, the con-

volution integral of the IRF and the change in radiative forcing yield the evolution of the global average temperature perturbation. Multiplying the latter with the first EOF that describes the spatial pattern of temperature yields the field of temperature perturbation.

2.6. Box-Type, Differential-Analogue Substitute Model

We have mapped the HRBM/CTBM onto a box-type, differential-analogue SM to include the effect of climate change on carbon storage. In the box-type model, the nonlinear dependence of respiration rates on climate can be included. This would not be possible with the linear IRF substitute. The box model is expressed in diagonal form [*Bolker et al.*, 1998] and the carbon balance of box i is

$$\frac{dN_i}{dt} = \frac{b_{i,0} \cdot exp(\beta_i \Delta T_{av})}{\sum_j b_{j,0} \cdot exp(\beta_j \Delta T_{av})} \cdot F_{\text{prod}} - k_{i,0} \cdot exp(\alpha_i \Delta T_{av}) \cdot N_i \quad (10)$$

where the quotient on the first line is further refered to as b_i and the first product on the second line as k_i. N_i is the carbon stock of box i. $b_{i,0}$ is the fraction of total productivity F_{prod} allocated into box i, and $k_{i,0}$ is the rate coefficient for respiration at the preindustrial reference temperature (ΔT_{av}=0). The denominator in the first right hand term is introduced to guarantee that the sum of all fractions is unity [$\sum_i b_i = 1$]. The coefficients b_i and k_i are assumed to depend exponentially on the global average surface temperature perturbation, ΔT_{av}; $k_{i,0}$, $b_{i,0}$ and their sensitivities to climate change, α_i and β_i , have been determined as described in section 3.5 and the appendix such that spatiotemporal changes in T, P, and cloud cover as captured by the first EOF-PC pairs are implicitly included.

We note that for fixed temperature the impulse response of the box model is readily computed as a sum of exponentials:

$$R_{\text{decay}}(t) = \sum_i b_i k_i \exp[-k_i t] \quad (11)$$

3. Results

3.1. Increase in Productivity in Response to Elevated CO_2

The first element that characterizes terrestrial carbon storage in response to rising atmospheric CO_2 is the increase in primary productivity. For the HRBM/CTBM, the relation between global NPP and atmospheric CO_2 (Figure 1) was calculated by increasing atmospheric CO_2 stepwise by 2 ppmv from 260 to 1274 ppmv, while keeping climate constant. For the FBM, the relations between GPP, NPP, and atmospheric CO_2 were determined by prescribing atmospheric CO_2 according to the IPCC WRE1000 scenario [*Schimel et al.*, 1996] following the observed concentration history from preindustrial CO_2 (278 ppmv) until today, then continuing to grow to finally approach stabilization at a level of 1000 ppmv. The ratio between NPP and GPP hardly changed over time in the FBM; it is 0.346. In the box-type biosphere of the Bern model, NPP depends logarithmically on atmospheric CO_2.

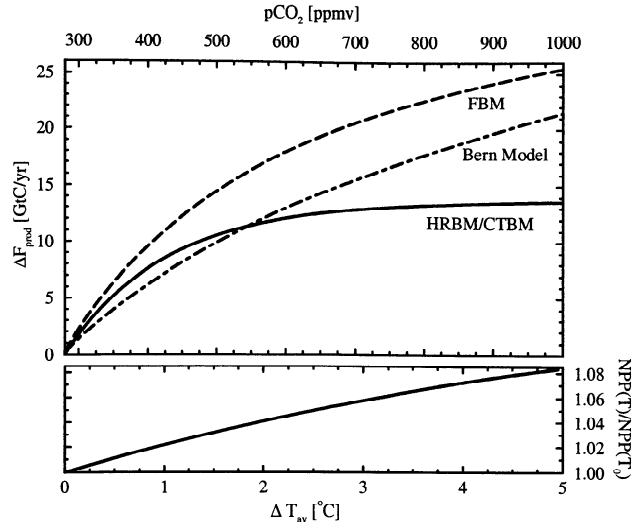

Figure 1. (top) Perturbation in Net Primary Productivity as a function of atmospheric CO_2, δF_{prod}, for the High-Resolution Terrestrial Biosphere Model/Community Terrestrial Biosphere Model (solid line), for the Frankfurt Biosphere Model (dashed line), the biosphere of the Bern model (dot-dashed line). (bottom) The Dependence of total NPP on changes in temperature, precipitation and cloud cover described by a dimensionless function of global average surface temperature ΔT_{av} for the HRBM/CTBM. Analytical representations of these productivity functions are provided on the Web (http:www.climate.unibe.ch/~joos/).

The global productivity functions of the three models reveal important differences (Figure 1). The strongest increase in productivity is found for the FBM, reaching 25 GtC yr^{-1} at CO_2 equal to 1000 ppmv. Primary productivity in the FBM grows over the entire range investigated, because the simulated increase in biomass and LAI supports additional productivity. The HRBM/CTBM simulates higher NPP than the Bern model, in the range of 280 to 600 ppmv. However, at higher CO_2 concentrations, NPP is larger in the Bern model than in the HRBM/CTBM. NPP in the HRBM/CTBM saturates toward 14 GtC yr^{-1} around 600 ppmv, because productivity is assumed to be limited by the inadequate supply of nutrients, whereas NPP in the Bern model increases over the investigated range of 280 to 1000 ppmv, although at a lower rate

than in the FBM. In a recent intercomparison of seven dynamic global vegetation models (DGVMs), it was found that the global NPP averaged for all DGVMs increased by around 35 GtC yr^{-1} in a scenario where CO_2 increased from the preindustrial level to 800 ppmv (http://www.pik-potsdam.de/posters.htm). Thus the sensitivity of NPP to rising CO_2 is lower for the FBM, the HRBM, and the Bern model than for the current ensemble of DGVMs.

3.2. Timescales of Carbon Overturning: Decay Impulse Response Function

The second element that characterizes terrestrial carbon storage in response to an increase in atmospheric CO_2 is the dynamics of carbon overturning in the biota, litter, and soils. This is characterized by the decay IRF determined as described in the appendix. A visual comparison of the decay IRF (Figure 2) shows that the general characteristics are similar for the three considered models, whereas significant differences exist in details. Respiration is highest in the first years after assimilation, and most of the assimilated carbon is respired within the first decades. The HRBM has very long-lived soil carbon pools in dry or cold areas (high latitudes, deserts), whereas such long-lived pools are hardly present in the FBM and not present in the Bern model. These features are also reflected in the IRFs. The IRFs of the FBM and Bern model approach zero values earlier than that of the HRBM/CTBM. In the next two sections, we will provide additional quantitative analyses of the IRFs and primary productivity functions.

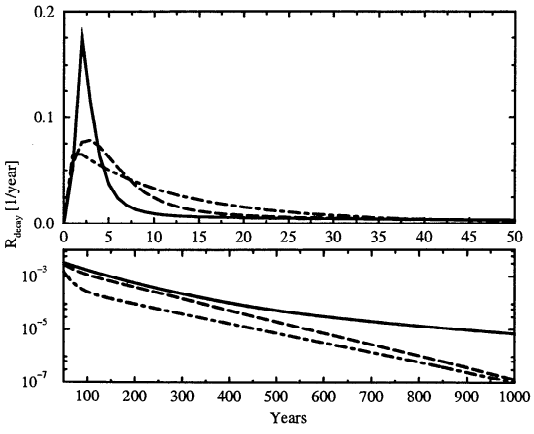

Figure 2. Response function characterizing the release of carbon into the atmosphere by heterotrophic respiration for the HRBM/CTBM (solid line), the FBM (dashed line), and the biosphere of the Bern model (dot-dashed line). Analytical representations of the response functions are provided on the Web (http:www.climate.unibe.ch/~ joos/).

3.3. Carbon Uptake Response to an Exponential Perturbation in Atmospheric CO_2

Atmospheric CO_2 has increased approximately exponentially since preindustrial time. For this simplified case, the carbon uptake response through CO_2 fertilization can be computed analytically from only two characteristic numbers. These are the Laplace transform of the decay IRF and the slope of the primary productivity as a function of atmospheric CO_2.

We linearize the relation between NPP and atmospheric CO_2. An inspection of Figure 1 shows that, at least for the models considered in the present study, the linear approximation is reasonable for atmospheric concentration values up to 500 ppmv. Then, the excess productivity ΔF_{prod} is a linear function with slope α of the excess atmospheric CO_2 concentration [$\Delta C(t) = C(t) - C(t_0)$]:

$$\Delta F_{\text{prod}}[C(t)] = \alpha \Delta C(t) \tag{12}$$

The net carbon flux into the biosphere, equation (2), can be written in this case as

$$F_{ab,\text{net}}(t) = F_{\text{prod},0}\ \alpha \left[\Delta C(t) - \int_{t_0}^{t} \Delta C(t') R_{\text{decay}}(t - t') dt'\right] \tag{13}$$

Assuming an exponentially increasing atmospheric CO_2 concentration, $\Delta C(t) \sim e^{\mu t}$, it is easy to show that the net biospheric uptake in this case results in

$$F_{ab,\text{net}}(t) = \Delta F_{\text{prod}}(t) \left[1 - \tilde{R}_{\text{decay}}(\mu)\right] \tag{14}$$

where $\tilde{R}_{\text{decay}}(\mu)$ denotes the Laplace transform of the IRF evaluated at the timescale of the exponential growth μ. $(1 - \tilde{R}_{\text{decay}}(\mu))$ is the fraction of assimilated excess carbon that is retained in the biosphere. If an analytical expression for the IRF is available in the form of a sum of exponentials, the Laplace transform is readily computed.

Equation (14) demonstrates the critical quantities that determine the terrestrial CO_2 uptake in the transient situation. These are (1) the excess productivity in response to the rising CO_2 concentration and (2) the fraction of assimilated carbon retained as measured by the Laplace transform of the decay IRF evaluated at μ.

An analysis of the atmospheric CO_2 concentration history since preindustrial times from ice core measurements shows that the timescale of the anthropogenic perturbation, μ^{-1}, lies between 30 and 40 years. Results for the terrestrial sink flux in the three models as computed from (14) for 1990 are given in Table 1. Compared with the Bern model, carbon sequestration levels in 1990 predicted by the IRF SMs of the HRBM/CTBM and the FBM are higher by a factor of 1.5 and 2.5, re-

Table 1. Biospheric Carbon Uptake in Response to a Small Exponential CO_2 Perturbation

	FBM	HRBM/CTBM	Bern Model
linear substitute model, GtC yr^{-1}	3.6	2.0	1.5
nonlinear substitute model, GtC yr^{-1}	2.9	1.8	1.2
$\tilde{r}_{\text{decay}}(\mu)$	0.46	0.64	0.63
$\Delta F_{\text{prod}}(1990)$, GtC yr^{-1}	6.6	5.6	4.1

The biospheric carbon uptake in response to CO_2 fertilization for the year 1990 was calculated by using a linearized form (equation 12) of the different impulse response function (IRF) substitute models. The histories of primary productivity and atmospheric CO_2 are assumed to be proportional to an exponential function, $e^{-\mu t}$. Then, the net biospheric carbon uptake at time t depends on the Laplace transform of the decay response function shown in Figure 2 evaluated at μ $[\tilde{r}_{\text{decay}}(\mu)]$ and the perturbation in primary productivity at t, $\Delta F_{\text{prod}}(1990)$. The exponential timescale of the perturbation μ was set to $1/35$ yr^{-1}, i.e., comparable to the timescale of the observed atmospheric concentration increase. The perturbation in net primary productivity was calculated for each model by evaluating the productivity function shown in Figure 1 for the observed atmospheric CO_2 concentration at 1990. For comparison, the carbon uptake for the year 1990 as obtained by prescribing the observed atmospheric CO_2 concentration history in the nonlinear pulse substitute model is shown as well. Abbreviations are defined as follows: FBM: Frankfurt Biosphere Model; HRBM/CTBM, High-Resolution Terrestrial Biosphere Model / Community Terrestrial Biosphere Model.

spectively. The large carbon sequestration of the FBM as compared with the HRBM and Bern models is due to both, a high excess productivity and a relatively slow respiration of assimilated carbon on the timescale of the atmospheric CO_2 increase. The small value of the Laplace transform for the FBM implies that a high percentage of the assimilated excess carbon is stored. On the other hand, the higher sequestration for the HRBM than for the Bern model is explained entirely by the stronger response of productivity to the increase of atmospheric CO_2 in the HRBM model, whereas the Laplace transforms, $\tilde{r}_{\text{decay}}(\mu)$, and thus the average dynamics of carbon overturning are almost identical for the two models on the timescale of the industrial perturbation.

Next, the decay IRFs are interpreted in terms of the classical age theory. In particular, we evaluate the ultimate capacity of the terrestrial biota to store anthropogenic carbon.

3.4. Response Functions, Age Theory, and the Ultimate Capacity for Carbon Storage

Next, the decay IRFs are interpreted in terms of the classical age theory. In particular, we evaluate the ultimate capacity of the terrestrial biota to store anthropogenic carbon.

3.4.1. Age distribution of respired carbon. The mean age or residence time $\overline{\tau}(t)$, e.g., of a flux leaving a reservoir, is defined as [*Bolin and Rodhe*, 1973]:

$$\overline{\tau}(t) = \int_0^\infty \sigma(t,\tau)\ \tau\ d\tau, \qquad (15)$$

where t is the chronological time and τ is the age. For this example, age is defined as the time a particle has spent in a reservoir until leaving it. Here $\sigma(t,\tau)$ is the fraction of the flux that, at time t, has an age in the interval $[\tau, \tau + d\tau]$; σ is an age distribution or age probability density function. In general, age distributions can describe the age of material in a reservoir, of a flux leaving the reservoir or of a flux entering the reservoir. The $\overline{\tau}(t)$ may then be interpreted as the mean age of all particles in a reservoir, as the average transit time of a flux leaving a reservoir, or as the average transit time (lifetime) of a flux entering a reservoir. As an example, for the human population these ages would correspond to the mean age of the living population at time t, the mean age of the people that die at year t, and the average expected lifetime of people that are born at year t.

The IRF R_{decay} is an age probability function. $R_{\text{decay}}(t-t')$ was defined in section 1 to represent the fraction of assimilated excess carbon that is respired at time t-t' after the assimilation (Figure 2). Thus we can interpret $(t-t')$ as an age τ and $R_{\text{decay}}(\tau)$ represents an age probability function, here assumed to be constant over the chronological time t. $R_{\text{decay}}(\tau)$ denotes the age distribution with respect to the average transit time through the biosphere of carbon that is assimilated owing to an increase in atmospheric CO_2. This is, in general, different from the age distribution of the respiration flux in preindustrial time. Thus R_{decay} refers explicitly to the perturbation in fluxes and stocks of carbon induced by the rise in atmospheric CO_2 relative to preindustrial conditions.

3.4.2. Ultimate uptake capacity of the biosphere. The mean transit time of excess carbon may be used to estimate the increase in carbon storage in a new equilibrium. This yields the ultimate or maximum capacity of the model to store additional carbon under a prescribed new atmospheric CO_2 concentration, assuming a constant climate. This maximum storage capacity is realized many centuries later, when all biospheric fluxes have reached their new constant equilibrium values and NPP equals heterotrophic respiration. The mean transit time of excess carbon, $\overline{\tau}_{\text{decay}}$, is then equivalent to the turnover time τ_0 of the carbon assimilated in excess to the pre-industrial assimilation rate. The turnover time is:

$$\overline{\tau}_{\text{decay}} = \tau_0(\text{anthrop. perturb.}) = \frac{\Delta N_\infty}{\Delta F_{\text{prod},\infty}}, \quad (16)$$

where ΔN_∞ is the stored excess carbon and $\Delta F_{\text{prod},\infty}$ is the perturbation in productivity at the new steady state.

We evaluated (16) to determine the uptake capacity ΔN_∞ for a stabilization of atmospheric CO_2 at twice the preindustrial value corresponding to an atmospheric CO_2 perturbation of 280 ppmv. Mean transit times of carbon allocated by NPP are ~59 years for the HRBM/CTBM, 45 years for the FBM, and 37 years for the Bern model (Table 2) as calculated by applying (15) and $R_{\text{decay}}(\tau)$ as age distribution. Multiplication of the transit time and the perturbation in NPP, $\Delta F_{\text{prod},\infty}$, yields an equilibrium carbon storage of 798 GtC (375 ppmv) for the FBM, 655 GtC (309 ppmv) for the HRBM/CTBM, and 432 GtC (203 ppmv) for the Bern model (Table 2). Thus the potential to store anthropogenic carbon is largest for the HRBM at a CO_2 concentration of 560 ppmv because of its very long-lived soil pools in high latitudes. The storage capacity will increase further for the FBM and the Bern model with increasing CO_2but will saturate at around 600 ppmv for the HRBM/CTBM as indicated in Figure 1.

The fraction of anthropogenic carbon that remains airborne at the new equilibrium is related to the uptake capacity. In an atmosphere-land biota-only system, the airborne fraction is defined as the ratio of the perturbation in atmospheric carbon inventory to the perturbation in the combined atmospheric and biospheric inventories. It is 43% for the FBM, 48% for the HRBM/CTBM, and 58% for the Bern biosphere. This is large compared with a typical equilibrium airborne fraction of 20% for an atmosphere-ocean [*Enting et al.*, 1994] and of 7% for an atmosphere-ocean-sediment system on a millennium timescale [*Archer et al.*, 1998]. This implies, that on long timescales, most of the excess carbon is stored in the ocean (including sediments), and only minor fractions are stored on land or remain in the atmosphere.

3.4.3. Turnover time for the preindustrial equilibrium. *Thompson et al.* [1996] applied preindustrial turnover times to estimate the ultimate uptake capacity of the biota. We calculated turnover times from the ratio of the total preindustrial carbon stock and preindustrial NPP to be 60 years for the HRBM/CTBM, 32 years for the FBM, and 37 years for the 4-box model (Table 2). The turnover time for preindustrial carbon is exactly the same as that for anthropogenic carbon in the case of the four-box biosphere, because the decay of organic carbon and allocation is time invariant. Similarly, the difference is very small for the HRBM/CTBM (59 versus 60 years). For the FBM, nonlinearities in the allocation scheme (see section 2.3) result in different turnover times for anthropogenic and preindustrial carbon. The fraction of assimilated carbon that is allocated in the relatively long-lived structural carbon pool (RC pool) increases with NPP, and the fraction that is allocated in the short-lived vegeta-

Table 2. Timescales of Biospheric Carbon and the Uptake Capacity of the Biosphere

	FBM	HRBM/CTBM	Bern Model
ΔN_∞ (560 ppmv), GtC	798	655	432
ΔF_{prod} (560 ppmv), GtC yr^{-1}	16.78	11.74	11.68
$\overline{\tau}_{\text{decay}}$ (anthropogenic carbon), years	45	59	37
τ_0 (preindustrial), years	32	60	37
$\overline{\tau}_{stock}$ (anthropogenic carbon), years	66	153	82

The ultimate uptake capacity of the biosphere to store anthropogenic carbon, ΔN_∞, in response to increasing CO_2 only is the product of the average transit time of anthropogenic carbon, $\overline{\tau}_{\text{decay}}$ and the increase in NPP, ΔF_{prod}, from the preindustrial steady state to a new steady state. Values are given for an assumed new atmospheric equilibrium concentration of 560 ppmv. The average transit time of anthropogenic carbon, $\overline{\tau}_{\text{decay}}$, and the mean age of the sequestered anthropogenic carbon at a new equilibrium, $\overline{\tau}_{\text{stock}}$, were calculated by applying the pulse decay response function shown in Figure 2 as age probability function. The overturning time for the preindustrial steady state, τ_0, was obtained by dividing the global carbon stock by global NPP.

tion pool (GC pool) decreases. Thus the turnover for anthropogenic carbon is substantially longer (45 years) than that for the total carbon in the system in preindustrial times (32 years). We conclude that preindustrial turnover times cannot be used, in general, to calculate the ultimate uptake capacity in response to CO_2 fertilization.

3.5. Box-Type Substitute Model for HRBM/CTBM

The parameters for a box-type SM to simulate carbon storage in response to CO_2 and climate as well as the dependence of NPP on climate and CO_2 have been determined from simulations with the spatially resolved HRBM/CTBM, where CO_2, T, P, and cloud cover fields were varied (see appendix). Thus the parameters of the box SM and NPP depend implicitly on regional climate change. Recall, however, that NPP and the coefficients of the SM depend formally only on the perturbation in global average surface temperature.

Global NPP is increasing at a rate of ~1.5% per degree warming in the HRBM/CTBM (Figure 1). Thus the changes in temperature, precipitation, and cloud cover stimulate productivity in the HRBM/CTBM.

Our optimal solution to represent the response of the HRBM to a global warming scenario is an SM that includes five reservoirs (Figure 3) with nominal overturning times of 0.2, 1.5, 9, 74, and 254 years. The pool with the overturning time of 0.2 years exhibits a small negative inventory at equilibrium. This is typical for models where material experiences transfer through successive reservoirs. The two short-lived pools can be easily combined to one reservoir (with positive inventory) for scenario calculations of the anthropogenic CO_2 transient. Thus, for typical timescales longer than a few years, the HRBM can be represented by four parallel reservoirs only.

The mean overturning time (or the inverse of the average rate coefficient for decomposition) is 59 years for preindustrial conditions and is therefore in agreement with the mean preindustrial overturning time of the HRBM/CTBM (60 years). Correspondingly, total preindustrial carbon stock of the box model is only 2% lower than that of the HRBM/CTBM (2510 GtC).

Next, we consider the effect of global warming on the global average rate coefficient for decomposition. Recall that the average rate coefficient is defined by the ratio of global respiration to global carbon stock. The response of the HRBM/CTBM to a warming climate is that (1) in general local respiration rates are increased and (2) a higher fraction of the total primary production is allocated into long-lived pools as compared to preindustrial climate caused by a stimulation of the productivity in high-latitudes where respiration rates are generally low. The first mechanism leads to an increase in the global average rate coefficient, whereas the second mechanism tends to decrease the global average rate coefficient as on average more carbon is found in pools with low respiration rates. Local respiration rates are reacting instantaneously to changing temperatures. However, the impact of changes in carbon allocation on carbon stocks and on global respiration evolves only slowly. Thus, the instantaneous change in the average respiration rate in response to a climate change is larger than that after the biosphere has approached its new equilibrium.

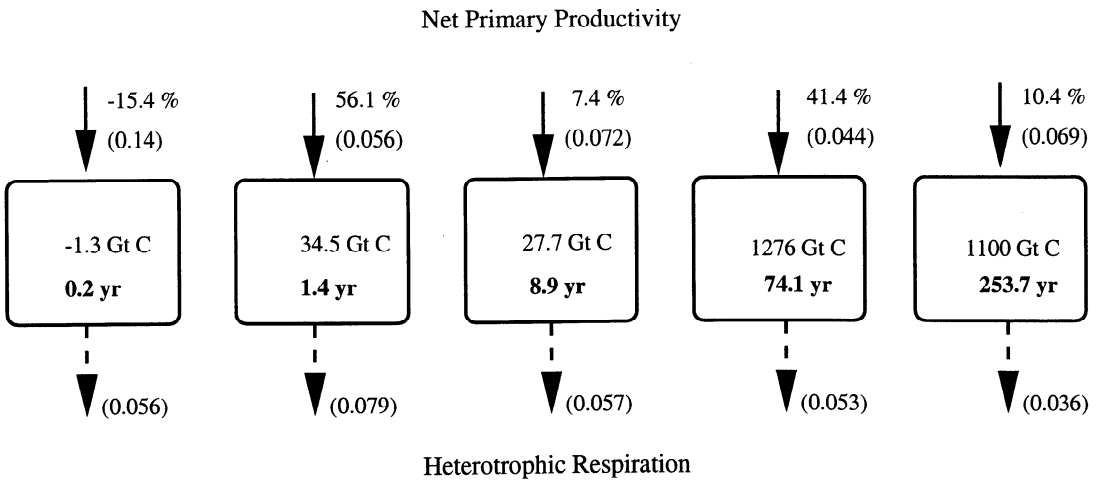

Figure 3. Structure of the box-type, differential-analogue substitute for the HRBM/CTBM. Preindustrial pool sizes and overturning times (bold line), $1/r_{i,0}$, are given in GtC and years. The fraction of NPP allocated into pool i at preindustrial equilibrium, $b_{i,0}$, is shown in percent. The temperature sensitivities of the respiration rates α_i and those of the allocation fractions β_i are shown in parentheses.

The instantaneous response to an increase in ΔT_{av} of 1°C is an increase in total respiration of 4.7% , whereas at the new equilibrium the average rate coefficient for respiration has decreased by only 2.8%. These values correspond to effective Q_{10} factors of 1.58 and 1.34, respectively.

At the new equilibrium, the decrease in overturning time relative to the preindustrial value is 2.8% for an increase in ΔT_{av} from 0°C to 1°C but only 2.0% for a step from 4°C to 5°C. This means that an additional temperature increase will result in almost 30% less carbon release at a temperature level of 5°C above the preindustrial steady state than at the preindustrial steady state when production is kept constant.

How will climate change affect the ultimate uptake capacity? The relative increase in carbon stock in response to a perturbation in climate and CO_2 is a function of the relative increase in productivity and the relative decrease in turnover time. It can be computed analytically for the new equilibrium by applying (17) and (18) and the productivity functions shown in Figure 1:

$$\frac{N_\infty(\Delta T_{\mathrm{av}}, \Delta \mathrm{CO}_2)}{N_0} = \frac{\tau_\infty(\Delta T_{\mathrm{av}})}{\tau_0} \frac{F_{\mathrm{prod}}(\Delta T_{\mathrm{av}}, \Delta \mathrm{CO}_2)}{F_{\mathrm{prod},0}} \tag{17}$$

At equilibrium, the overturning time is the sum over all boxes of the products of allocation fractions b_i and individual overturning times τ_i:

$$\tau_\infty(\Delta T_{\mathrm{av}}) = \sum_i b_i(\Delta T_{\mathrm{av}}) \tau_i(\Delta T_{\mathrm{av}}) \tag{18}$$

It is found that the ultimate uptake capacity is decreased by 6 to 20% by the impact of climate change as compared to the uptake capacity in response to CO_2 fertilization only in scenarios where atmospheric CO_2 is stabilized between 450 and 1000 ppmv (Table 3). In summary, the HRBM/CTBM exhibits a relatively low sensitivity to climate change, because NPP is increased and more carbon is allocated into long-lived pools in a warmer climate as compared with preindustrial conditions.

3.6. Anthropogenic CO_2 Transient

We have run the IPCC stabilization scenarios S450, S650, and WRE1000 [*Schimel et al.*, 1996] to further illustrate the differences in the terrestrial carbon storage between the three models, and to test the response of the SMs as compared with the spatially resolved models. Atmospheric CO_2 is prescribed according to the observed concentration history until the present, then continues to grow until it approaches stabilization at levels of 450, 650, and 1000 ppmv, respectively.

First, we consider the case where climate is kept constant. Then, the models sequester between 300 and 500 GtC (S450), between 500 and 800 GtC (S650), and between 700 to 1000 GtC (WRE1000) until year 2300 (Table 3). Maximum annual uptake is between 3 and 5 GtC yr^{-1} for WRE1000 (Figure 4). It is noted that the

Table 3. Cummulative Carbon Storage for the Period 1765 to 2300 and at Equilibrium

	S450		S650		WRE1000	
	1765-2300	Uptake Capacity	1765-2300	Uptake Capacity	1765-2300	Uptake Capacity
			Varying CO_2			
FBM	505 (0.1%)	550	784 (1.5%)	880	996 (1.3%)	1130
Bern Model	304	310	516	520	719	780
HRBM/CTBM	474 (0.5%)	547	618 (0.7%)	738	678 (2.6%)	850
			Varying Climate and CO_2			
HRBM/CTBM	445	514	560	662	578	681

The cumulative carbon uptake for the period from years 1765 to 2300 was obtained by applying the pulse substitute of the Bern model, the FBM, and the HRBM/CTBM in response to increasing CO_2 only, as well as for the box substitutes of the HRBM/CTBM in response to CO_2 and climate change. Deviations between results obtained with the spatially resolved models and their pulse substitutes are given in parentheses. Atmospheric CO_2 has been prescribed according to observations until 1990 and then following the Intergovernmntal Panel on Climate Change scenarios S450, S650, and WRE1000, where the atmospheric CO_2 concentration is stabilized at 450, 650 and 1000 ppmv, respectively. The related climate change was calculated by employing a nonlinear pulse substitute of the European Center/Hamburg Model 3 / Large Scale Geostrophic Ocean General Circulation Model coupled Atmosphere Ocean General Circulation Model to force the box substitute of the HRBM/CTBM. The ultimate uptake capacity, i.e., the carbon storage that will be realized when the biosphere has reached equilibrium, is given for comparison. Depending on the model and the scenario, 80 to 98% of the uptake capacity has been realized until the year 2300.

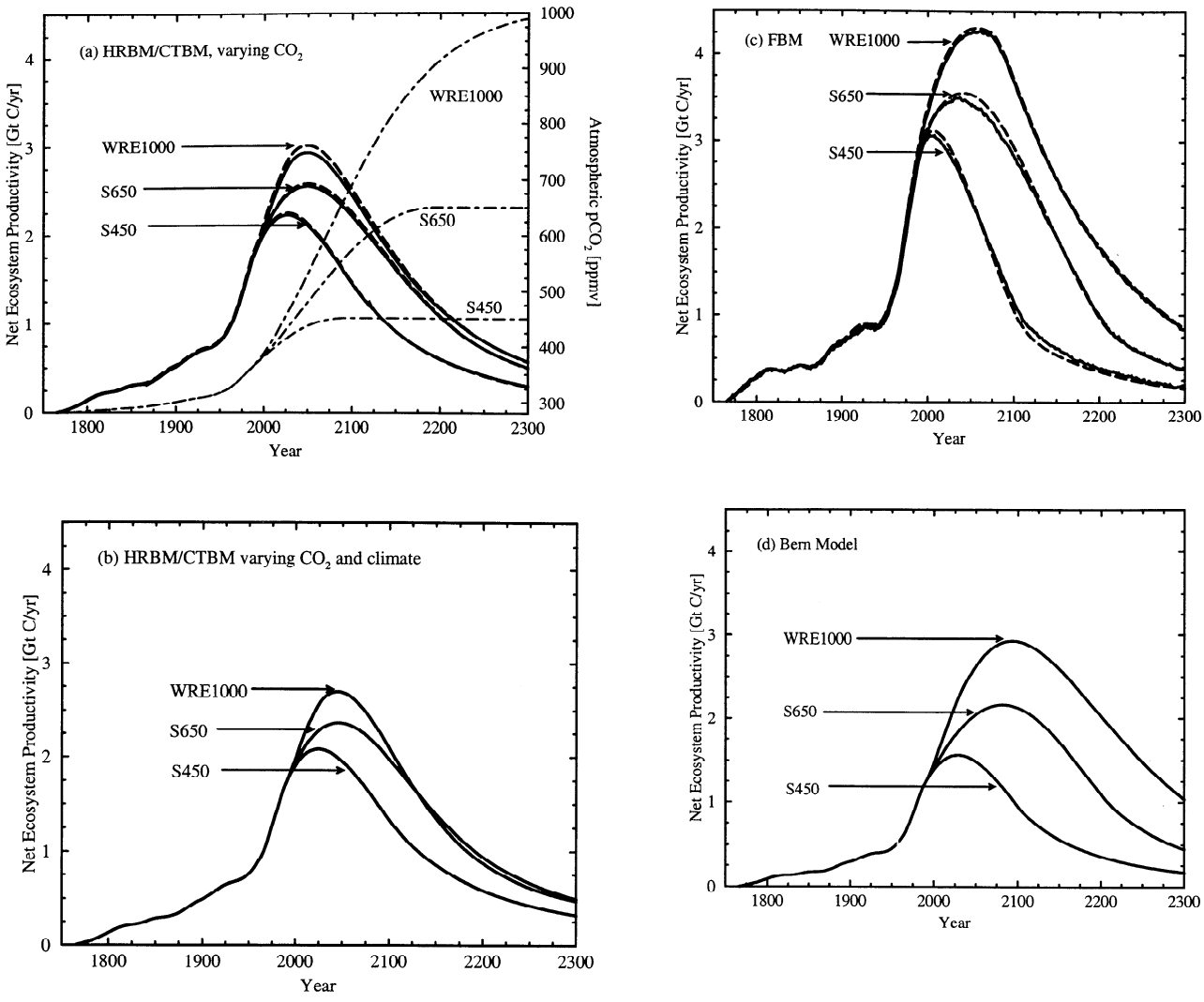

Figure 4. Net ecosystem productivity (NEP) as simulated by the (a) HRBM/CTBM (solid line) and (b) in response to both increasing CO_2 and climate change, (c) NEP as simulated by FBM (solid line) and (d) the Bern model, and their pulse substitutes (dashed line) in response to elevated CO_2 only. Atmospheric CO_2 was prescribed in the models according to the Intergovernmental Panel on Climate Change stabilization scenarios S450, S650, and WRE1000 where CO_2 is stabilized at 450, 650, and 1000 ppmv (dot-dashed line). For the box substitute of the HRBM/CTBM, climate change was calculated by employing a nonlinear pulse substitute of the European Center/Hamburg Model 3 / Large Scale Geostrophic Ocean General Circulation Model coupled Atmosphere Ocean General Circulation Model.

maximum uptake occurs well before atmospheric CO_2 reaches its maximum. NEP starts to decrease around the time where the growth rate in atmospheric CO_2 (and in NPP) starts to decline, i.e. when the second derivative with respect to time of the CO_2 curve turns negative [*Kohlmaier et al.*, 1998]. For the FBM and the Bern model, 90% and more of the ultimate uptake capacity has been realized until year 2300, whereas for the HRBM model only, 80-85% of the equilibrium storage is reached at year 2300.

The FBM sequesters more carbon than the HRBM and the Bern model (Figure 4). The differences between FBM and HRBM in carbon storage for the periods from 1765 to 2300 are small for the scenario S450 and reach almost 50% when CO_2 is stabilized at 1000 ppmv (WRE1000). The small difference between HRBM and FBM for stabilization at 450 ppmv (S450) can be understood by the slow approach to equilibrium of the HRBM and a higher uptake capacity of HRBM than FBM at 450 ppmv. For high CO_2 concentrations, both

the high uptake capacity of the FBM and its relatively fast realization explain the high cumulative uptake of the FBM. Carbon storage is lowest for the Bern model, except for WRE1000.

Second, both climate and CO_2 were varied for the HRBM/CTBM. Global average temperature perturbation was projected using the IRF representation of ECHAM3/LSG and an equilibrium warming for a CO_2 doubling ($\Delta T_{2\times}$) of 2.5°C. For the S450, S650, and WRE1000 CO_2 profiles, climate change reduced the cumulative uptake for the period from 1765 to 2300 by 6 to 14% (Figure 4 and Table 3). Thus terrestrial carbon storage in the HRBM/CTBM is relatively insensitive to global climate change, because the carbon loss by increased soil respiration rates is partly compensated by the increase in NPP in response to global warming (Figure 1).

Differences in global NEP simulated by the spatially resolved models and their IRF SMs are small. For the HRBM, deviations in the annual net terrestrial uptake are always smaller than 0.9% (S450), 1.6% (S650), and 2.7% (WRE1000) (Figure 4). For the FBM, differences in annual NEP are generally small and always less than 8% . The differences in the cumulative biospheric carbon uptake for the period from 1765 to 2300 are always smaller than 2.4% for both the HRBM and the FBM (Table 3).

To compare the box SM and the HRBM, we analyzed results of the 850 year transient $4xCO_2$ climate change scenario where atmospheric CO_2 increases exponentially in the first 120 years. The deviation in total cumulative uptake between HRBM/CTBM and its box-type SM is 3.5% and maximal deviation in NEP is 0.1 GtC yr^{-1} between the two models. Furthermore, we also find small deviations in NEP simulated by the HRBM/CTBM, its IRF-SM, and its box-type SM for constant climate.

3.7. Carbon Isotopes ^{13}C and ^{14}C

As a further application of the SMs (see (3) and (4)), we calculate the uptake of bomb-produced ^{14}C and the difference in the $\delta^{13}C$ signature of assimilated and respired carbon, i.e., the $\delta^{13}C$ disequilibrium. The $\delta^{13}C$ disequilibrium and the isotopic flux related to it need to be known in inversion studies of the atmospheric $\delta^{13}C$ signal to deduce the partitioning of oceanic and terrestrial carbon sinks [e.g., *Keeling et al.*, 1989; *Joos and Bruno*, 1998; *Joos et al.*, 99 a]. In 1990, the modeled air-biota disequilibrium was $0.45^0/_{00}$ with respect to heterotrophic respiration and the disequilibrium flux was $20^0/_{00}$ GtC yr^{-1} in a simulation with the IRF-SM of the HRBM/CTBM. This is in agreement with results obtained by the HRBM/CTBM [*Wittenberg and Esser*, 1997]. The prescribed atmospheric $\delta^{13}C$ history is based on a spline-fit to the observations [*Francey et al.*, 1999] with a cutoff period of 4 years to remove short-term fluctuations [*Joos et al.*, 99 a]. For the IRF SM of the FBM, the disequilibrium flux was $32^0/_{00}$ GtC yr^{-1} in 1990. The low fluxes of the HRBM/CTBM are in line with results obtained for the Carnegie-Ames-Stanford Approach biosphere model (CASA) [*Thompson and Randerson*, 1999], whereas the FBM results are in line with box model estimates [*Francey et al.*, 1995; *Joos and Bruno*, 1998] and disequilibrium fluxes constrained by O_2/N_2 data [*Rayner et al.*, 1999].

The budget of bomb-produced radiocarbon provides an additional constraint on the global carbon cycle [*Hesshaimer et al.*, 1994; *Joos*, 1994]. The atomic bomb tests in the late 1950s to early 1960s added a substantial amount of radiocarbon to the natural background. Once test ban treaties were set in place, atmospheric concentrations decreased as bomb radiocarbon became absorbed by the ocean and biosphere. Atmospheric explosions were rare after 1963, so that the global radiocarbon budget should have remained roughly constant. However, present estimates of the ^{14}C budgets that are based on simple terrestrial box models [e.g., *Joos and Bruno*, 1998] exhibit a considerable imbalance for the post test ban period. Simulated terrestrial uptake for the period from 1965 to 1989 is 109 x 10^{26} atoms for the SM of the HRBM/CTBM and 99 x 10^{26} atoms for the SM of the FBM. This is similar to the uptake estimated by the Bern model (90 x 10^{26} atoms). Our results suggest that the consideration of spatially resolved biota models does not lead to a substantial revision of present budget estimates.

We tested, for the HRBM/CTBM, how well isotopic fluxes are represented by the IRF SMs and found very good agreement between the two model versions. For example, the ^{13}C /^{12}C in heterotrophic respiration decreased by $0.796^0/_{00}$ between 1765 and 1990 as modeled by the HRBM/CTBM, while the maximum deviation in $\delta^{13}C$ of the heterotrophic respiration between the HRBM/CTBM and its IRF SM is $0.036^0/_{00}$, and the average deviation (1765-1990) is $0.0065^0/_{00}$. The difference in the cumulative uptake of bomb-produced radiocarbon for the period from 1955 to 1990 is very small, i.e., 0.18%.

4. Discussion and Conclusion

There exists considerable evidence that the present day decadal average net atmosphere-to-biosphere flux is small [*Siegenthaler and Oeschger*, 1987; *Keeling et al.*, 1996; *Heimann and Maier-Reimer*, 1996; *Bruno and Joos*, 1997; *Joos et al.*, 99 a; *Rayner et al.*, 1999]. This implies that emissions by land use changes and deforestation [*Houghton*, 1993] must be compensated by a terrestrial sink. However, the magnitude of the land use flux and therefore the magnitude of the compensating sink flux are highly uncertain [*Schimel et al.*,

1996]. The mechanisms responsible for the sink flux are under debate. Here we have applied models that tackle the potential response in carbon storage to increasing CO_2 and warming climate only. Other factors, such as changes in land use and associated emissions and regrowth, fire frequencies, species composition feedbacks, adaption, or the effect of additional nitrogen loadings, have been neglected. Many studies of the sensitivities of production to increased atmospheric CO_2 suggest an enhancement of plant productivity. However, it is not clear to what extent carbon storage is indeed stimulated on an ecosystem or global level. The uncertainty of how productivity will respond in the future to increasing CO_2 is reflected in the different relationship between global NPP and CO_2 found for the FBM, the HRBM/CTBM, and the Bern model. It is also a consensus view that soil respiration will increase with warmer climate. How NPP will respond to climate change probably depends strongly on the future patterns of temperature and precipitation. The different timescales of carbon overturning found for the FBM, the HRBM/CTBM, and the Bern model suggest that more work is needed to better quantify terrestrial carbon dynamics and to improve its representation in models.

The results of the scenario calculations where CO_2 is stabilized at 450, 650, or 1000 ppmv may be viewed in the context of the present debate on the saturation of the terrestrial sink. Our results demonstrate quantitatively three limiting mechanisms for carbon storage: (1) NEP decreases when the growth rate of atmospheric CO_2 or, more exactly, the growth rate of NPP decreases. In the three considered models maximum NEP is reached well before the maximum CO_2 level. (2) Cumulative carbon storage will not further increase with increasing CO_2 if NPP has already reached its saturation level, as illustrated by the similar cumulative uptake obtained with the HRBM/CTBM for the scenario stabilizing at 650 and 1000 ppmv. (3) Global warming leads to an increased soil respiration and a reduction in carbon storage.

How do our results compare with the current set of emerging dynamical global vegetation models? Carbon sequestration in response to CO_2 fertilization is, on average, higher in the DGVMs than in the HRBM/CTBM, whereas the percentage reduction in storage caused by global warming is higher in the DGVMs than in the HRBM/CTBM. Then for a comparable CO_2 climate change scenario, a similar amount of carbon is stored on average in the HRBM/CTBM as in the DGVMs for a comparable CO_2 climate change scenario (http://www.pik-potsdam.de/posters.htm).

The complexities of the climate system and the tools used to represent subsystems such as the terrestrial biota necessitate for many applications a simpler description in a condensed form. We have mapped the spatially resolved HRBM/CTBM and FBM to simple global SMs for simulations of carbon storage in response to rising CO_2 and climate change. Our results demonstrate also that models that exhibit a complex and nonlinear behavior can be rather well represented by SMs. The work presented here is viewed as a further step toward a comprehensive SM for global change applications, which features the dynamics of spatially resolved, state-of-the-art models. The terrestrial SMs developed in this study are part of a substitute model [*Joos et al.*, 1996; *Joos and Bruno*, 1996; *Hooss et al.*, 1999] that describes the redistribution of anthropogenic carbon between the atmosphere-ocean-biosphere system and the response of the global mean temperature and other climate variables to an increase in radiative forcing as mediated by CO_2 and other agents.

SMs are cost-efficient and permit important sensitivity calculations. They are easy to implement and require only modest computer resources. Carefully designed SMs are accurate as compared with their parent models. These features make them especially well suited for statistical analyses, applications in integrated assessment studies and cost-benefit analyses, and scenario calculations such as those performed in the assessments of the Intergovernmental Panel on Climate Change, which require the coupling of climate and biogeochemical models to address climate biogeochemical cycle feedbacks. For the interpretation of results obtained with SMs, however, it is important to recall that SMs share the strengths and deficiencies of their parent models.

SMs provide important diagnostics. For example, the expected average transit time of anthropogenic carbon, the fraction of assimilated carbon retained for an exponential CO_2 transient, or the ultimate uptake capacity are readily derived from the IRF.

The IRF may also be used as a convenient measure to compare the global overturning time scales of terrestrial biosphere models [*Joos et al.*, 1996; *Thompson and Randerson*, 1999]. In addition, the box SM approach yields an average climate sensitivity of carbon overturning, e.g. expressed as an effective global Q_{10} factor. This sensitivity is another useful measure to evaluate and compare the response of global terrestrial models to anthropogenic climate change.

On the other hand, SMs also have limitations. Most importantly, they can adequately represent the dynamics of the parent complex model only for the perturbations and the time scales for which the SM has been optimized. This limitation becomes especially critical if the complex model show strong non-linearities and thresholds. Clearly, the SM's derived here have shown to provide valid responses for global change scenario calculations in which atmospheric CO_2 ranges between

about 280 and 1000 ppmv. However, they may not mimic the parent complex model if driven e.g. by glacial atmospheric CO_2 levels. Likewise, the climate sensitive substitute model derived from the HRBM/CTBM only captures the dynamics of the terrestrial carbon reservoir to the transient, decadal to centennial global warming pattern as simulated by a particular climate model and not the response to short term natural climate fluctuations, such as e.g. the El Niño-Southern Oscillation.

It must also be acknowledged, that the terrestrial carbon cycle models included in the present study are of intermediate complexity. The relative success in representing their global dynamics with simpler SMs evidently provides not guarantee, that the approach will also work in the case of dynamical global vegetation models. Nevertheless, because of the advantages of SMs as outlined above, a similar investigation with more complex terrestrial models might be very valuable. Clearly, such a study might also include other impact factors, such as changes in land use and nutrient input, and it might cover additional climatic forcing factors (e.g. insolation) possibly also represented by more than one spatial pattern.

Appendix

A.1. Determination of Impulse Response Functions

A.1.1. HRBM/CTBM. The global IRF of the HRBM/CTBM has been determined by a pulse-like carbon input into the assimilation pools of the HRBM/CTBM during 1 year. This was done by increasing the atmospheric CO_2 concentration above its equilibrium value by 10 or 100 ppmv during 1 year only. The two experiments yielded identical normalized IRFs. The perturbation in annual global respiration was monitored for the next 1000 years and then normalized to obtain the global decay IRF (Figure 2). This procedure was feasible, as the response of the HRBM to a pulse is independent of the size of the pulse.

A.1.2. FBM. The decay IRF for the FBM was determined from results of the IPCC WRE1000 scenario. We did not use an impulse experiment to determine the IRF because the highly nonlinear allocation and phenology schemes of the FBM yield a response to a pulse-like perturbation that is not representative of the timescales of the anthropogenic CO_2 transient. The perturbations in global (autotrophic and heterotrophic) respiration, $\Delta F_{\mathrm{resp}}(\mathrm{FBM}, t)$, and global GPP, $\Delta F_{\mathrm{GPP}}(\mathrm{FBM}, t)$, have been calculated with the spatially resolved model for the period from 1765 to 2300. The square of the difference between the total respiration as calculated by the FBM and that by the convolution integral of the SM was used as a cost function:

$$\sum_{t=1765}^{2300} \left[\begin{array}{l} \Delta F_{\mathrm{resp}}(\mathrm{FBM}, t) - \\ \sum_{t'=1765}^{t} \Delta F_{\mathrm{GPP}}(\mathrm{FBM}, t') R_{\mathrm{decay}}(t - t') \Delta t' \end{array} \right]^2 \tag{A1}$$

A nonlinear fit algorithm based on the Levenberg Marquardt method [*Press et al.*, 1989] was used to determine the unknown global IRF $R_{\mathrm{decay}}(t)$ by minimizing the cost function. We constrained the solution by assuming that the IRF can be represented as a sum of exponentials. This assumption is justified based on the dynamics of the spatially resolved FBM. This procedure did not lead to numerical problems. The time step $\Delta t'$ in the second sum of (A1) is 1 year. The resulting IRF is related to GPP and corresponds to an effective response that implicitly includes nonlinearities associated with the assimilation and allocation of carbon in the FBM. The IRF is representative for the timescales of the anthropogenic perturbation. For comparison with the HRBM and the Bern model, we calculated also the IRF that is related to NPP. This is done by setting the decay IRF for GPP to zero during the first year that results almost entirely from autotrophic respiration. Subsequent normalization yields the decay response for NPP (Figure 2). For the Bern model, the IRF has been obtained analytically [*Joos et al.*, 1996].

A.2. Determination of the Parameters of the Box Substitute Model and Dependence of NPP on Climate and CO_2

A.2.1. NPP. The relation between NPP and the perturbation in climate and CO_2 was determined from an 850 year HRBM/CTBM simulation where the output from the 850 year transient 4× CO_2 simulation with the ECHAM3/LSG AOGCM is used. In the HRBM/CTBM, we prescribed as boundary conditions the first PCs and EOFs for the perturbation in T, P, cloud cover and the related CO_2 concentrations of the ECHAM3/LSG simulation. The NPP simulated by the HRBM/CTBM was then approximated as the product of two analytical functions (Figure 1). The first function is the relation between NPP and CO_2 as determined in section 3.1. The second function depends on the global surface temperature perturbation (ΔT_{av}) only and describes the modification of NPP for changing patterns of T, P, and cloud cover. The calculated values for NPP are indistinguishable from the output of the HRBM/CTBM.

A.2.2. Rate coefficients. The preindustrial pool sizes and rate coefficients of the box-type SM described in section 2.6 were determined such as to minimize the deviation in (squared) global heterotrophic respiration between the HRBM/CTBM and the SM. We applied the CO_2 pulse scenario (section 3.2), where atmospheric CO_2 was increased during 1 year only and climate was kept constant, for the minimization.

To determine the temperature sensitivities α_i and β_i of the rate coefficients and allocation factors of the differential-analogue SM, the first EOFs for T, P, and cloud cover changes are applied as boundaries in the spatially resolved HRBM/CTBM. Temperature, cloud cover, and precipitation pattern were changed stepwise each 800 years in the HRBM/CTBM. Fifteen steps were applied that covered a range in the perturbation of global mean temperature (ΔT_{av}) from 0°C to 5°C. Then, the deviation between the (squared) respiration fluxes modeled by the HRBM/CTBM and the box SM were minimized to determine all sensitivities (Figure 3).

Acknowledgments. This work was founded by the Carbon Cycle Model Linkage Project (CCMLP) of the Electrical Power Research Institute (Palo Alto) and the Swiss National Science Foundation. We thank W. Cramer and R. Leemans for sharing their climatology and the participants of the CCMLP project for many stimulating discussions. We also thank the Deutsches Klima Rechenzentrum (DKRZ), Hamburg for computational support.

References

Archer, D., H. Kheshgi, and E. Maier-Reimer, Dynamics of fossil fuel CO2 neutralization by marine $CaCO_3$, *Global Biogeochem. Cycles, 12*, 259–276, 1998.

Bolin, B., and H. Rodhe, A note on the concepts of age distribution and transit time in natural reservoirs, *Tellus, 25*, 58–62, 1973.

Bolker, B. M., S. W. Pacala, and W. J. Parton, Linear analysis of soil decomposition: Insights from the century model, *Ecol. Appl., 8*, 425–439, 1998.

Bruno, M., and F. Joos, Terrestrial carbon storage during the past 200 years: A Monte Carlo analysis of CO_2 data from ice core and atmospheric measurements, *Global Biogeochem. Cycles, 11*, 111–124, 1997.

Cao, M., and F. I. Woodward, Dynamic responses of terrestrial ecosystem carbon cycling on global climate change, *Nature, 393*, 249–251, 1998.

Cramer, W., D. Kicklighter, A. Bondeau, B. M. III, G. Churkina, B. Nemry, A. Ruimy, and A. Schloss, Comparing global models of terrestrial net primary productivity (npp): Overview and key results., *Global Change Biol., 5*, 1 – 15, 1999.

Emanuel, W. R., G. G. Killough, W. M. Post, and H. H. Shugart, Modeling terrestrial ecosystems in the global carbon cycle with shifts in carbon storage capacity by land-use change, *Ecology, 65*, 970–983, 1984.

Enting, I. G., T. M. L. Wigley, and M. Heimann, Future emissions and concentrations of carbon dioxide: Key ocean/atmosphere/land analyses, Tech. Rep. 31, *CSIRO*, Atmos. Res., Melbourne, Victoria, 1994.

Esser, G., Sensitivity of global carbon pools and fluxes to human and potential climatic impacts, *Tellus, Ser. B, 39*, 245–260, 1987.

Esser, G., Osnabrück biosphere model: Construction, structure, results, in *Modern Ecology, Basic and Applied Aspects*, edited by G. Esser and D. Overdick, pp. 679–710, Elsevier Sci., New York, 1991.

Esser, G., I. Asselmann, and H. Lieth, Modelling the carbon reservoir in the system compartment "litter", in *Mitteilungen des Geologisch-Palaöntologischen Instituts der Universität Hamburg*, vol. *52*, pp. 39–58, Univ. of Hamburg, Hamburg, Germany, 1982.

Esser, G., J. Hoffstadt, F. Mack, and U. Wittenberg, High resolution biosphere model, documentation, model version 3.00.00, in *Mitteilungen aus dem Institut für Plflanzenökologie der Justus-Liebig-Universität Giessen*, vol. *2*, Univ. of Giessen, Germany, 1994.

Farquhar, G. D., S. von Caemmerer, and J. A. Berry, A biochemical model of photosynthetic CO_2 assimilation in leaves of C_3 species, *Planta, 149*, 78–90, 1980.

Farquhar, G. D., J. R. Ehleringer, and K. T. Hubick, Carbon isotope descrimination and photosynthesis, *Ann. Rev. Plant Physiology Mol. Biol., 40*, 503–537, 1989.

Francey, R. J., P. P. Tans, C. E. Allison, I. G. Enting, J. W. C. White, and M. Troller, Changes in oceanic and terrestrial carbon uptake since 1982, *Nature, 373*, 326–330, 1995.

Francey, R. J., C. E. Allison, D. M. Etheridge, C. M. Trudinger, I. G. Enting, M. Leuenberger, R. L. Langenfelds, E. Michel, and L. P. Steele, A 1000 year high precision record of $\delta^{13}C$ in atmospheric CO_2, *Tellus, Ser. B, 51*, 170–193, 1999.

Hasselmann, K., S. Hasselmann, R. Giering, V. Ocaña, and H. von Storch, Optimization of CO_2 emissions using coupled integral climate response and simplified cost models. A sensitivity study., *Tech. Rep. 192*, Max-Planck Institut für Meteorologie, Hamburg, Germany, 1996.

Haxeltine, A., and I. Prentice, Biome3: An equilibrium terrestrial biosphere model based on ecophysiological constraints, resource availability and competition among plant functional types., *Global Biogeochem. Cycles, 10*, 693 – 709, 1996.

Heimann, M., and E. Maier-Reimer, On the relations between the oceanic uptake of CO_2 and its carbon isotopes, *Global Biogeochem. Cycles, 10*, 89–110, 1996.

Heimann, M. et al., Evaluation of terrestrial carbon cycle models through simulations of the seasonal cycle of atmospheric CO_2: First results of a model intercomparison study, *Global Biogeochem. Cycles, 12*, 1–24, 1998.

Hesshaimer, V., M. Heimann, and I. Levin, Radiocarbon evidence for a smaller carbon dioxide sink than previously believed, *Nature, 370*, 201–203, 1994.

Hooss, G., R. Voss, K. Hasselmann, E. Maier-Reimer, and F. Joos, A non-linear impulse response model of the coupled carbon cycle-ocean-atmosphere climate system, *Tech. Rep. 290*, Max-Planck Institut für Meteorologie, Hamburg, Germany, 1999.

Houghton, J. T., L. G. M. Filho, B. A. Callander, N. Harris, A. Kattenberg, and K. Maskell, *Climate Change 1995-The Science of Climate Change: Contribution of WGI to the Second Assessment Report of the Intergovernmental Panel on Climate Change*, Cambridge Univ. Press, New York, 1996.

Houghton, R. A., Changes in terrestrial carbon over the last 135 years, in *The Global Carbon Cycle*, vol I15, edited by M. Heimann, pp. 139–157, Springer-Verlag, New York, 1993.

Indermühle, A. et al., Holocene carbon-cycle dynamics based on CO_2 trapped in ice at taylor dome, Antarctica, *Nature, 398*, 121–126, 1999.

Janecek, A., G. Benderoth, M. K. G. Lüdeke, J. Kindermann, and G. H. Kohlmaier, Model of the seasonal and perennial carbon dynamics in decidous-type forrests controlled by climatic variables, *Ecol. Modell., 49*, 101–124, 1989.

Joos, F., Imbalance in the budget, *Nature, 370*, 181–182, 1994.

Joos, F., and M. Bruno, Pulse response functions are cost-efficient tools to model the link between carbon emissions, atmospheric CO_2 and global warming, *Phys. Chem. Earth, 21*, 471–476, 1996.

Joos, F., and M. Bruno, Long-term variability of the terrestrial and oceanic carbon sinks and the budgets of the carbon isotopes ^{13}C and ^{14}C, *Global Biogeochem. Cycles, 12*, 135–150, 1998.

Joos, F., M. Bruno, R. Fink, T. F. Stocker, U. Siegenthaler, C. Le Quéré, and J. L. Sarmiento, An efficient and accurate representation of complex oceanic and biospheric models of anthropogenic carbon uptake, *Tellus, Ser. B, 48*, 397–417, 1996.

Joos, F., R. Meyer, M. Bruno, and M. Leuenberger, The variability in the carbon sinks as reconstructed for the last 1000 years, *Geophys. Res. Lett., 26*(10), 1437, 1999a.

Joos, F., G. Müller-Fürstenberger, and G. Stephan, Correcting the carbon cycle representation: How important is it for the economics of climate change?, *Envviron. Modell. Assess.*, in press, 1999b.

Kattenberg, A., F. Giorgi, H. Grassl, G. A. Meehl, J. Mitchell, R. Stouffer, T. Tokioka, A. Weaver, and T. Wigley, Climate models - Projections of future climate, in *IPCC Second Scientific Assessment of Climate Change*, edited by J. Houghton et al., pp. 285–357, Cambridge Univ. Press, New York, 1996.

Keeling, C. D., R. B. Bacastow, A. F. Carter, S. C. Piper, T. P. Whorf, M. Heimann, W. G. Mook, and H. Roelofzen, A three-dimensional model of atmospheric CO_2 transport based on observed winds, 1, Analysis of observational data, in *Aspects of Climate Variability in the Pacific and the Western Americas, Geophys. Monogr. Ser., vol. 55*, edited by D. H. Peterson, pp. 165–237, AGU, Washington, D. C., 1989.

Keeling, R. F., S. C. Piper, and M. Heimann, Global and hemispheric CO_2 sinks deduced from changes in atmospheric O_2 concentration, *Nature, 381*, 218–221, 1996.

Kicklighter, D. W. et al., A first order analysis of the potential role of CO_2 fertilization to affect the global carbon budget: A comparison study of four terrestrial biosphere models, *Tellus, Ser. B, 51*, 343–366, 1999.

Kindermann, J. et al., Structure of a global and seasonal carbon exchange model for the terrestrial biosphere. The frankfurt biosphere model (fbm), *Water Air Soil Pollut., 70*, 675–984, 1993.

Kirschbaum, M. U. F., A modelling study of the effects of changes in atmospheric CO_2 concentration, temperature and atmospheric nitrogen input on soil organic carbon storage, *Tellus, Ser. B, 45*, 321–334, 1993.

Kohlmaier, G. et al., The Frankfurt biosphere model: A global process oriented model for the seasonal and longterm CO_2 exchange between terrestrial ecosystems and the atmosphere, II; global results for potential vegetation in an assumed equilibrium state, *Clim. Res., 8*, 1997.

Kohlmaier, G. H., C. Häger, F. Ift, G. Würth, F. Joos, and M. Bruno, Future development of the carbon cycle: The role of the biota/forests within the IPCC stabilization scenarios, in *Carbon Dioxide Mitigation in Forestry and Wood Industry*, edited by G. H. Kohlmaier, M. Weber, and R. A. Houghton, pp. 269–291, Springer-Verlag, New York, 1998.

Leemans, R., and W. Cramer, The IIASA climate database for land areas on a grid with 0.5° resolution, *Res. Rep. RR-91-18.*, Int. Inst. for Appl. Syst. Anal. Laxenburg, Austria, 1991.

Lüdeke, M. K. B. et al., The Frankfurt Biosphere Model: A global process-oriented model of seasonal and long-term CO_2 exchange between terrestrial ecosystems and the atmosphere, I, Model description and illustrative results for cold deciduous and boreal forests, *Clim. Res., 4*, 143–166, 1994.

Lüdeke, M. K. B., S. Dönges, R. D. Otto, J. Kindermann, F.-W. Badeck, P. Ramge, U. Jäkel, and G. H. Kohlmaier, Response in NPP and carbon stores of the northern biomes to a CO_2-induced climatic change, as evaluated by the Frankfurt biosphere model (FBM), *Tellus, Ser. B, 47*, 191–205, 1995.

Maier-Reimer, E., and K. Hasselmann, Transport and storage of CO_2 in the ocean - an inorganic ocean-circulation carbon cycle model, *Clim. Dyn., 2*, 63–90, 1987.

McGuire, A. D., J. M. Melillo, L. A. Joyce, D. W. Kicklighter, A. L. Grace, B. Moore III, and C. J. Vorosmartyr, Interactions between carbon and nitrogen dynamcis in estimating net primary productivity for potential vegetation in North America, *Global Biogeochem. Cycles, 6*, 101–124, 1992.

Melillo, J. M., A. D. McGuire, D. W. Kicklighter, B. Moore III, C. J. Vorosmarty, and A. L. Schloss, Global climate change and terrestrial net primary production, *Nature, 363*, 234–240, 1993.

Nemry, B., L. Francois, J.-C. Gerard, A. Bondeau, and M. Heimann, Comparing global models of terrestrial net primary productivity (NPP): analysis of the seasonal atmospheric CO2 signal, *Global Change Biol., 5*, 1999.

Oeschger, H., and M. Heimann, Uncertainties of predictions of future atmospheric CO_2 concentrations, *J. Geophys. Res., 88*, 1258–1262, 1983.

Orr, J. C., Ocean carbon cycle model intercomparison project (OCMIP), phase 1 (1995-1997), Rep. 7, Int. Geosphere Biosphere Program / Glob. Anal. Interpretation and Modell., Univ. of New Hampshire, Durham, 1999.

Potter, C. S., J. T. Randerson, C. B. Field, P. A. Matson, P. M. Vitousek, H. A. Mooney, and S. A. Klooster, Terrestrial ecosystem production: A process model based on global satellite and surface data, *Global Biogeochem. Cycles, 7*, 811–841, 1993.

Prentice, C., W. Cramer, S. P. Harrison, R. Leemans, and R. A. Monserud, A global biome model based on plant physiology and dominance, soil properties and climate, *J. of Biogeogr., 19*, 117–134, 1992.

Press, W. H., B. P. Flannery, S. A. Teukolsky, and W. T. Vetterling, *Numerical Recipes*, Cambridge Univ. Press, New York, 1989.

Rayner, P. J., I. G. Enting, R. J. Francey, and R. Langenfelds, Reconstructing the recent carbon cycle from atmospheric CO_2, $\delta^{13}C$ and O_2/N_2 observations, *Tellus, Ser. B, 51*, 213–232, 1999.

Sarmiento, J. L., J. C. Orr, and U. Siegenthaler, A perturbation simulation of CO_2 uptake in an ocean general circulation model, *J. Geophys. Res., 97*, 3621–3645, 1992.

Schimel, D., I. Enting, M. Heimann, T. Wigley, D. Raynaud, D. Alves, and U. Siegenthaler, CO_2 and the carbon cycle, in *Climate Change 94, Radiative Forcing of Climate Change*, edited by J. T. Houghton et al., pp. 38–71, Cambridge Univ. Press, New York, 1994a.

Schimel, D., B. Braswell, E. Holland, R. McKeown, D. Ojima, T. Painter, W. Parton, and A. Townsend, Climatic, edaphic and biotic controls over storage and turnover of carbon in soils, *Global Biogeochem. Cycles, 8*, 1994b.

Schimel, D., D. Alves, I. Enting, M. Heimann, F. Joos, D. Raynaud, and T. Wigley, CO_2 and the carbon cycle,

in *IPCC Second Scientific Assessment of Climate Change*, edited by J. Houghton, pp. 76–86, Cambridge Univ. Press, New York, 1996.

Schimel, D., M. Grubb, F. Joos, R. K. Kaufmann, R. Moos, W. Ogana, R. Richels, and T. Wigley, Stabilisation of atmospheric greenhouse gases: Physical, biological, and socio-economic implications, *IPCC Tech. Pap. III*, Intergov. Panel on Clim. Change, Geneva, 1997.

Shine, K., R. G. Derwent, D. J. Wuebbles, and J.-J. Morcrette, Radiative forcing of climate, in *Climate Change: The IPCC Scientific Assessment*, edited by J. T. Houghton, G. J. Jenkins, and J. J. Ephraums, pp. 41–68, Cambridge Univ. Press, New York, 1990.

Siegenthaler, U., and F. Joos, Use of a simple model for studying oceanic tracer distributions and the global carbon cycle, *Tellus, Ser. B, 44*, 186–207, 1992.

Siegenthaler, U., and H. Oeschger, Predicting future atmospheric carbon dioxide levels, *Science, 199*, 388–395, 1978.

Siegenthaler, U., and H. Oeschger, Biospheric CO_2 emissions during the past 200 years reconstructed by deconvolution of ice core data, *Tellus, Ser. B, 39*, 140–154, 1987.

Thompson, M., and J. Randerson, Impulse response functions of terrestrial carbon cycle models: Method and application, *Global Change Biol., 5*, 371–394, 1999.

Thompson, M., J. T. Randerson, C. M. Malmström, and C. B. Field, Change in net primary production and heterotrophic respiration: How much is necessary to sustain the terrestrial carbon sink?, *Global Biogeochem. Cycles, 10*, 711–726, 1996.

Wittenberg, U., and G. Esser, Evaluation of the isotopic disequilibrium in the terrestrial biosphere by a global carbon isotope model., *Tellus, Ser. B, 49*, 263–269, 1997.

G. Esser and U. Wittenberg, Institute for Plant Ecology, Justus-Liebig-University, Heinrich-Buff-Ring 38, D-35397 Giessen, Germany. (Gerd.Esser@bot2.bio.uni-giessen.de, Uwe.Wittenberg@bot2.bio.uni-giessen.de)

M. Heimann, Max-Planck-Institut fuer Biogeochemie, Tatzendpromenade 1a, D-07701 Jena, Germany. (martin.heimann@bgc-jena.mpg.de)

G. Hooss, W. Sauf, and R. Voss, Max-Planck-Institut fuer Meteorologie, Bundesstrasse 55, D-20146 Hamburg, Germany. (hooss@dkrz.de, sauf@dkrz.de, k204007@blitz.dkrz.de)

G. Kohlmaier, Institut für physikalische und theoretische Chemie (IPTC), J.W. Goethe Universität, Marie Curie Strasse 11, 60439 Frankfurt am Main, Germany. (g.kohlmaier@chemie.uni-frankfurt.de)

R. Meyer and F. Joos, Physics Institute, University of Bern, Sidlerstrasse 5, CH-3012 Bern, Switzerland. (meyer@climate.unibe.ch; joos@climate.unibe.ch)

(Received June 16, 1998; revised May 17, 1999;
accepted June 4, 1999.)